Materials and Design 77 (2015) 149–160

Contents lists available at ScienceDirect

Materials and Design

journal homepage: www.elsevier.com/locate/matdes

Effects of solid lubricants, load, and sliding speed on the tribological behavior of silica reinforced composites using design of experiments

T. Ram Prabhu

Center for Military Airworthiness and Certification, Marathalli Colony Post, Bangalore, India

ARTICLE INFO

Article history:
Received 2 January 2015
Revised 25 March 2015
Accepted 28 March 2015
Available online 28 March 2015

Keywords:
Wear and friction
Copper composites
Analysis of variance
Solid lubricants
Regression analysis

ABSTRACT

In the present study, the effects of solid lubricants, braking load and sliding speed on the tribological behavior of Cu/silica composites were investigated using design of experiments and statistical methods. Three types of composites were prepared using different types of solid lubricants (h-BN, graphite, and MoS_2) by powder metallurgy. The wear and friction behavior of the composites were evaluated for a range of braking loads (300, 600, and 900 N) and sliding speeds (3, 6, and 9 m/s) in a subscale dynamometer. The composites were characterized for density, hardness, microstructure, wear surface morphology and surface roughness properties. A statistical model was developed to identify the significant factors affecting the wear resistance of the composites. The key findings of our study are: (1) MoS_2 reinforced composites possess the highest density, densification, hardness, and lowest surface roughness among the composites, (2) MoS_2 is the most effective lubricant in improving the wear resistance of the composites for the selected experimental domain, (3) Amongst the solid lubricant, brake load and sliding speed, the solid lubricant is the most significant factor affecting the wear resistance of the composites, (4) graphite reinforced composites provide higher braking performance at 3 m/s for all loading conditions whereas both h-BN and MoS_2 reinforced composites provide better braking performance among composites at higher speed (>3 m/s) and load (>300 N) conditions.

1. Introduction

Brake friction composites demand diverse physical, mechanical and thermal properties because of the complex process of sliding. The essential requirements are high wear resistance, high friction, superior thermal stability and conductivity, low heat expansion coefficient, high stiffness, high fracture toughness and high strength [1–4]. Some of these properties are contradictory, and usually do not coexist in a homogenous material, for example, the wear resistance and the friction coefficient, and the strength and the toughness. Therefore, the brake materials need to be designed with the right amount of diverse constituents to optimize these properties.

Particle reinforced metal matrix composites (MMC_p) are suitable materials for brake friction materials applications [4–9]. These composite materials have the application in the low (<500 kJ) and medium energy (<5 MJ) brakes. They have the potential to replace the currently used low life polymer based brake pads in the automobiles and high cost carbon based brake discs in the military aircrafts. MMC_ps have the capability to provide incompatible properties by simply combining constituents of diverse properties. A typical MMC_p has two main constituents: the matrix and the reinforcement. The matrix is intended to provide toughness, corrosion resistance, high thermal conductivity and melting point properties. Among the metallic elements, copper appears to be a most suitable matrix material because of the benefits of high melting point (1080 °C), high thermal conductivity (400 W/m K), good machinability, high toughness, excellent corrosion resistance, and low thermal expansion properties. There were many wear studies reported on the Cu matrix composites [10,11]. Further, most of wear studies on Cu based MMC_ps and other matrix materials such as Fe and Al based MMC_ps were performed at low speed (0.5–5 m/s) and load (2–50 N) conditions [10–16]. Literature on the high sliding speed and load effects on the wear and friction properties of the Cu based MMCs is limited [5].

The ceramic particles are aimed at improving the thermal stability, hardness, strength, wear resistance, and friction properties. Among various ceramic particles, SiC, B_4C, and Al_2O_3 are widely used with the metal matrix owing to their compatibility with the common matrix materials (Fe, Cu and Al) and easy availability [17]. Silica is another potential ceramic particle that has not been explored widely so far [18]. Silica has many advantages over SiC and B_4C. It is the cheapest reinforcement [19]. It has relatively less

E-mail address: ramprabhu.t@gmail.com

http://dx.doi.org/10.1016/j.matdes.2015.03.059
0261-3069/

abrasive effect on the die during compaction and tools during machining and hence provides longer die/tool life than other reinforcements. It has near zero thermal expansion (0.55×10^{-6}/°C) and lower density (2.1 g/cc) than other reinforcements[19]. It has got excellent corrosion, chemical and thermal shock resistance [20]. It is stable in the metallic matrix especially in copper and does not react with the matrix during sintering. Hence, the bonding between the matrix and particles is expected to be better than other reinforcements. In contrast, carbides react with matrix materials and dissociate at elevated temperature resulting in poor interface bonding quality [21–23]. Most of the studies on silica reinforced MMCs are based on mechanical properties evaluation [20,24–26]. There are relatively very few wear studies on the silica reinforced MMCs. For instance, Rohatgi et al. [18] have developed composites of Al alloy (A206 grade)/silica with different silica contents (0–13 wt%) for the tribological applications. They reported that the higher amount of silica deteriorates the wear rate and friction coefficient of composites due to an incompatibility between the Al matrix and silica. Probably, silica and Cu have better compatibility. However, there are no studies reported on the Cu/silica composites.

Apart from the matrix and ceramic particles, an additional constituent usually present in the friction material is the solid lubricant. The purpose of the lubricant addition is to stabilize the friction and wear during the braking process [27]. Graphite is the most common lubricant used in the friction material. The principal advantages of the graphite are that it has good lubricity, high thermal conductivity, high damping capacity, protection of counter surface against excessive wear by involving in forming tribofilm and excellent seizure resistance [17,28]. Besides graphite, other lubricants such as h-boron nitride (h-BN), MoS_2, Sb_2S_3, Cu_2S find widespread use in the friction materials. There are some studies focused on understanding the lubricant effects on the wear and friction properties of polymer based automobile friction materials [27,29]. These reports conclude that the lubricants help in forming a friction film at the pad-disc interface that improves the friction and wear resistance. The presence of many ingredients (filler, binder, fiber, abrasive, lubricants, friction modifiers and so on) in a polymer based friction material makes it difficult to understand the effect of solid lubricants on the wear and friction properties. To the best of our knowledge, similar studies on MMCs are not found in the literature. Therefore, there is a knowledge gap in understanding the effect of lubricants on the tribological behavior of MMC_p.

Models are generally developed to study the effects of mechanical (load, speed, and sliding distance) and constituent (particle size, shape, amount, and type, and abrasive grit size) factors on the tribological behavior of MMCs. Most of the wear models in the literature are finite element models combined with the Archard law and physical based models. The main limitations of these models are that (1) they do not provide information on the combined effects of factors, (2) they are also mostly qualitative in nature, and (3) the predictive capability of the models is usually limited [30,31]. On the other hand, models based on statistics are emerging recently. In statistical models, the techniques such as means and *S*/*N* ratio analysis, analysis of variance, artificial neural network and genetic algorithms are utilized to study the experimental data [32,33]. The advantages of these models are that (1) they explain the statistical and physical significance of the input factors, (2) they provide predictive equations of reasonable accuracy for the selected experimental domain, and (3) they help to understand the interaction between the input variables on the output. Numerous investigators have developed statistical models for Al/SiC, Zn (ZA 27) alloys and steels [12–16,34–36]. They used analysis of variance and linear regression techniques to study the interaction of various factors (load, speed, sliding distance, particle type and size, and abrasive grit size) on the wear resistance of composites.

In light of the above facts, the work is designed as follows: first, Cu/silica composites with various solid lubricants (graphite, h-BN, and MoS_2) were processed by powder metallurgy. These composites were tested for wear and braking behaviors under the spectrum of braking loads (300–900 N) and sliding speeds (3–9 m/s). The wear data were analyzed statistically to identify the significant factor influencing the wear resistance of the composites. Finally, the effects of solid lubricants, load and speed on the braking behavior of composites were also studied.

2. Experimental procedure

2.1. Materials and processing

The powders of copper, silica, MoS_2, graphite, h-BN were used to prepare the composites. The characteristics of the powders are presented in Table 1.

Initially, three batches of Cu/20 vol% silica mix were prepared in a double cone blender. These batches were mixed with different solid lubricant of 10 vol% (MoS_2 or graphite or h-BN) to form three separate mixtures. The composition of the mixtures is given in Table 2. These mixtures were cold compacted at a compaction load of 600 kN in a single uniaxial compaction press. The diameter and thickness of the compacts were 30 mm and 5 mm respectively. The green compacts were sintered in a bell furnace under the hydrogen gas reducing atmosphere. The sintering cycle is given in Fig. 1. In order to further improve the dimensional accuracy and to close the surface pores in the compacts, the sintered compacts were again pressed at a load of 800 kN.

2.2. Factorial experimental design

A factorial approach was used to study the factors affecting wear resistance of the composites. The experiments were designed using the Taguchi method. This method is simple, robust, efficient and systematic in designing experiments. Detailed information about the Taguchi method is given elsewhere [37,38]. In the present study, it is planned to study the influence of three factors (*P*) (braking load, braking speed, and type of solid lubricant labeled as *L*, *S*, and *X* respectively) on wear resistance of the composites. The solid lubricant was treated as a categorical variable whereas the speed and the load are considered as continuous variables. Three levels (*n*) (upper, base, and lower labeled as 1, 2, and 3 respectively) were considered in each factor, as shown in Table 3. A standard L_{27} orthogonal array was selected to plan our experiments. According to this scheme, there were 27 experiments and

Table 1
Properties of the powders.

Powder	Silica	Graphite	h-BN	MoS_2	Copper
Mean size (μm)	50–125	150–160	106–150	44–60	75–106
Purity (min)	99.5%	95%	99.8%	98.5%	99%
Apparent density (g/cc)	–	2.2	0.78	–	2–2.4
Grade	Fused silica	Natural (flaky)	Hexagonal type	–	Electrolytic

Table 2
Chemical composition of the composites.

Elements (vol.%)	G	B	M
Copper	80%	80%	80%
Silica	10%	10%	10%
Graphite	10%	–	–
h-Boron nitride	–	10%	–
MoS_2	–	–	10%

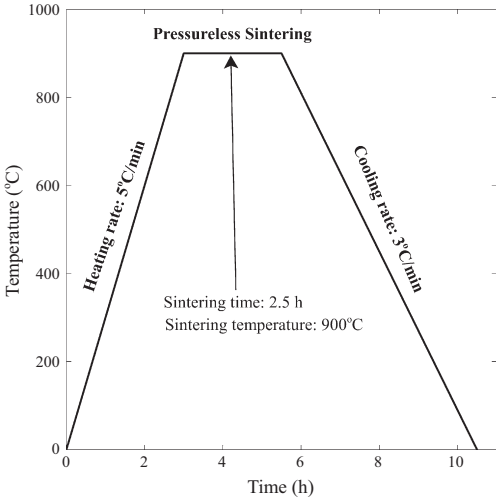

Fig. 1. Pressureless sintering cycle.

Table 3
Level of variations in the experimental testing parameters.

Level	Type of solid lubricant, *X*	Load, *L* (N)	Braking speed, *S* (m/s)
1	Graphite (G)	300	3
2	h-BN (B)	600	6
3	MoS_2 (M)	900	9

no two factors were common in any of the experiments. Thus, the unique effects of any factor could be obtained. Table 4 gives the experimental plan according to the L_{27} orthogonal array. The array has 27 rows and 3 columns indicating factors and their level. The experiments were conducted as per the orthogonal array with level of factors given in each array row. The data collected from the experiments were analyzed using the statistical methods to study the wear loss response with the criterion of minimum mass loss which in turn implies the product life and performance.

2.3. Testing

The density of the composites was measured by the Archimedes principle. Three samples were tested for density in each composite and the average value was reported. The average porosity content of the composites was determined from the following relation:

$$v_f = \frac{\rho_t - \rho_e}{\rho_t}, \quad (1)$$

where v_f, the porosity content, ρ_t, theoretical density calculated from the rule of mixture, and ρ_e, the measured density from the Archimedes principle. The hardness of the composites was measured in a Brinell scale (Wolpert universal hardness tester) using a 10 mm steel ball and 100 N load. Ten hardness readings were taken from each composite. The average value was reported as a hardness of the composite. The particle size range of the powders

Table 4
L_{27} orthogonal array experimental design.

Test	Solid lubricant type	Speed (m/s)	Load (N)
1	Graphite	3	300
2	Graphite	3	600
3	Graphite	3	900
4	Graphite	6	300
5	Graphite	6	600
6	Graphite	6	900
7	Graphite	9	300
8	Graphite	9	600
9	Graphite	9	900
10	h-BN	3	300
11	h-BN	3	600
12	h-BN	3	900
13	h-BN	6	300
14	h-BN	6	600
15	h-BN	6	900
16	h-BN	9	300
17	h-BN	9	600
18	h-BN	9	900
19	MoS_2	3	300
20	MoS_2	3	600
21	MoS_2	3	900
22	MoS_2	6	300
23	MoS_2	6	600
24	MoS_2	6	900
25	MoS_2	9	300
26	MoS_2	9	600
27	MoS_2	9	900

was determined using the sieve analysis. The BS 410 standard was used to convert the mesh number into the particle size. The microstructure of the composites was characterized in an optical microscope (Nikon Epiphot). A Obsnap surface roughness tester (TR200) was used to measure the surface roughness of the composites. The tester uses a diamond stylus of 10 μm diameter and has 0.01 μm precision.

The wear and braking parameters (coefficient of friction, stopping distance, stopping time, and mean torque) were evaluated in a subscale disc-on-pad dynamometer at room temperature and 70% humidity conditions. The dynamometer setup simulates a typical flat on flat sliding condition. The schematic of the stator pad and rotor disk combination in a typical dynamometer is shown in Fig. 2 The operating procedure of the dynamometer, and sample preparation techniques for the brake test were reported in our previous reports [39,40]. A gray cast iron disc (Grade: AMTY 273-68, C: 3–3.6%, Si: 1.6–2.3%) of 500 mm diameter was used as a rotor in the dynamometer. The surface roughness and hardness of the rotor were 3–4 μm and 225 BHN respectively. The brake testing parameters are shown in Table 5. Fifty braking stops were simulated to collect sufficient braking parameters data for each composite.

The samples were cleaned with acetone before and after the brake test. The weight of the samples was measured in a digital balance (precision = 0.1 mg). The wear loss was determined as the difference between the sample weights before and after the test. The weight loss of the disc was not considered in this study because of the fact that the hardness of the steel disc (420 BHN) was higher than that of the composites. A stereo binocular microscope (SEIWA) was used to characterize the wear surface morphology of the composites.

2.4. Statistical methods

A three-way analysis of variance (ANOVA) method was used to study the influence of solid lubricants, load, and speed on the wear resistance of the composites. In this method, the following equations were used to calculate the *F* ratio.

$$CF = \frac{\left(\sum y^2\right)^2}{x.l.s.n} \quad (2)$$

$$SS_x = \frac{\left(\sum X\right)^2}{l.s.n} - CF \quad (3)$$

$$SS_l = \frac{\left(\sum L\right)^2}{x.s.n} - CF \quad (4)$$

$$SS_s = \frac{\left(\sum S\right)^2}{x.l.n} - CF \quad (5)$$

$$SS_{x.l} = \frac{\left(\sum X \cdot L\right)^2}{n} - SS_x - SS_l - CF \quad (6)$$

$$SS_{x.s} = \frac{\left(\sum X \cdot S\right)^2}{n} - SS_x - SS_s - CF \quad (7)$$

$$SS_{l.s} = \frac{\left(\sum L \cdot S\right)^2}{n} - SS_l - SS_s - CF \quad (8)$$

$$SS_{x.l.s} = \frac{\left(\sum X \cdot L \cdot S\right)^2}{n} - SS_x - SS_l - SS_s - SS_{x.l} - SS_{x.s} - SS_{l.s} - CF \quad (9)$$

$$SS_T = \left(\sum y^2\right) - CF \quad (10)$$

$$Error = SS_T - SS_x - SS_l - SS_s - SS_{x.l} - SS_{x.s} - SS_{l.s} - SS_{x.l.s} \quad (11)$$

$$MS = SS/df \quad (12)$$

$$F = MS/MS_{Error} \quad (13)$$

where *CF*, *SS*, *MS*, and *df* denote the correction factor, sum of squares, mean of squares, and degrees of freedom respectively. $\sum X, \sum L$, and $\sum S$ are the sum of totals representing the solid lubricant type, load and speed respectively. Indices representing the levels in the solid lubricant type, load and speed are *x*, *l*, and *s* respectively. *n* and *y* denote the total number of experiments ($n = 27$) and the wear loss response (by mass (mg)) in each experiment respectively. The subscript *T* denotes the treatment of each factor.

Table 5
Testing parameters for the brake tests.

Braking speed (m/s)	Load (N)	Braking energy (kJ)	Moment of Inertia of the flywheel (N ms^{-2})	Speed of rotor (rpm)
3	300	1550	20	120
6	600	6200	20	240
9	900	13,175	20	350

The high *F* ratio from the analysis indicates the most significant factor influencing the wear loss. The analysis was performed to a confidence level of 95%.

The mean analysis was also performed to identify the factors influencing the wear process. Further, the experimental results were converted to signal to noise ratios (*S*/*N*). The smaller *S*/*N* ratio – the better characteristic criterion was selected to study the significant factors influencing the wear resistance because the lower wear loss indicates the better life and performance of the material. The *S*/*N* ratio (dB) was calculated using the following logarithmic function.

$$S/N = -10 \log\left[\left(\sum y^2\right)/n\right] \quad (14)$$

where *y* is the response (wear loss) data, and *n* is the total number of observations. The response tables for the mean analysis and the *S*/*N* ratio analysis were generated to rank the factors.

3. Results and discussion

3.1. Microstructure, physical and mechanical properties

The microstructure of the composites is shown in Fig. 3. First, we look at the ceramic particle distribution and the bonding characteristics in the composites. The uniform distribution of the ceramic particles (silica) ensures isotropic properties and uniform distribution of stresses in the composites. The morphology of the silica particles is found to have an irregular shape in the composites. There are no evidences of particle clustering zones, and defects (pores, microcracks and debonding) at the particle/matrix interfaces. It is noted that the region around the silica particles is smooth and free from interfacial reaction products indicating strong mechanical bonding between the matrix and particles. Next, we look at the solid lubricant distribution in the composites. G type composites (as shown in Fig. 3(a)) have graphite in the form

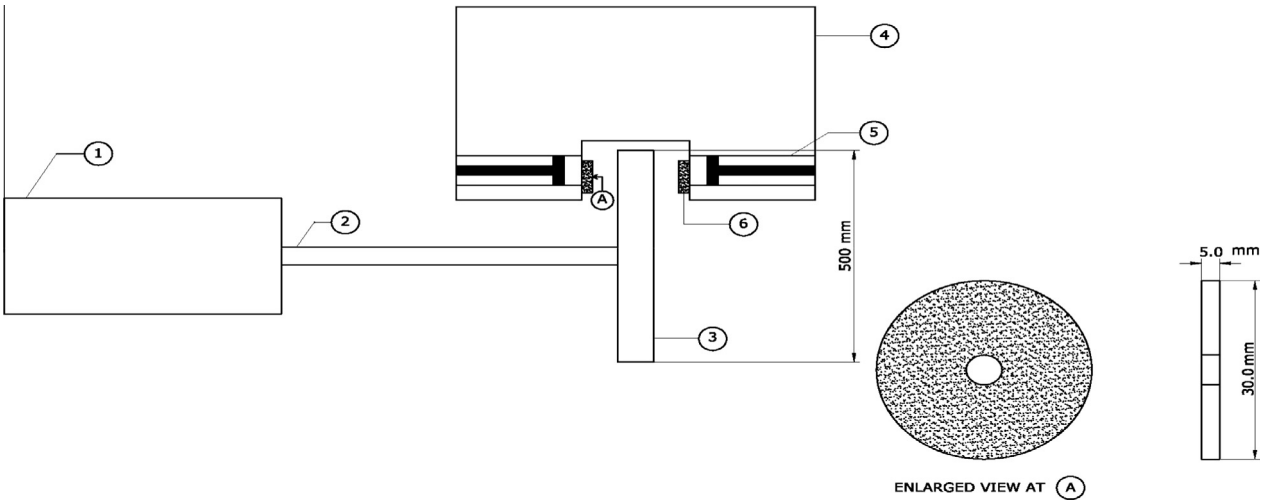

Fig. 2. Schematic of the dynamometer, (1) motor, (2) flywheel, (3) gray cast iron rotor, (4) brakepad holder, (5) brake piston, and (6) brakepad composite. The thickness and diameter of the composite pad are 5 mm and 30 mm respectively. The distance between the pad axis and the disk rotation axis is 205 mm.

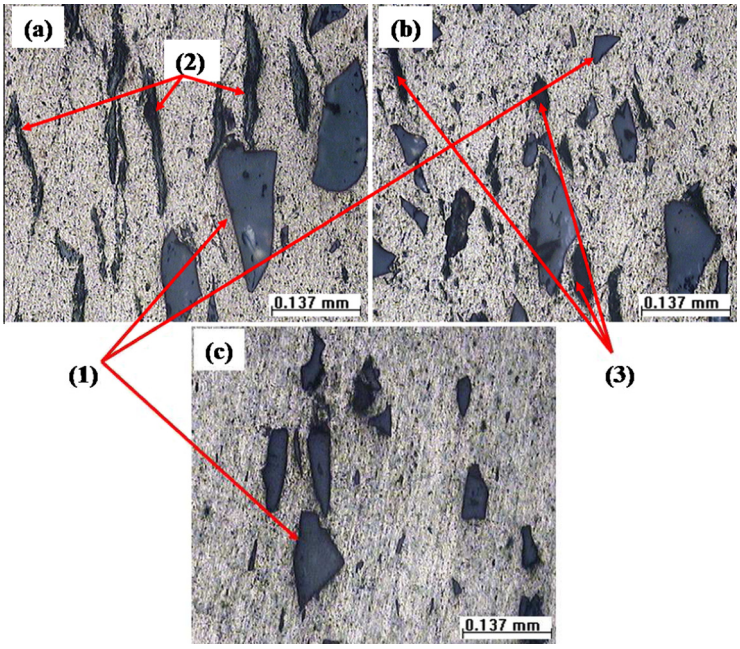

Fig. 3. Microstructures of (a) graphite reinforced (b) h-BN reinforced, and (c) MoS_2 reinforced Cu/silica composites. (1) Silica, (2) graphite flakes, and (3) h-BN particles.

of flakes distributed uniformly in the matrix. Similarly, B type composites (as shown in Fig. 3(b)) have a homogenous distribution of h-BN in the matrix. These observations suggest that both the graphite and the h-BN do not undergo any reaction with the matrix or ceramic particles during the sintering process. The MoS_2 particles are not distinguishable in the M type composites (as shown in Fig. 3(c)). It is probably because of their fine size (44–60 μm) and similar contrast with the matrix.

Other important observations from the microstructure of a B type composite (as seen in Fig. 3(b)) are clusters of tiny porosity close to the silica particles and the cracked silica particles. The high porosity content of a B type composite is attributed to these pore clusters. The compaction load would have cracked the particles. The cracked particles are potential sites for delamination crack nucleation during the wear. Also, they do not support the braking load during the wear process resulting in poor wear resistance, as will be discussed in detail in the next section.

The density, hardness and surface roughness, and % porosity of the composites are reported in Table 6. The effect of solid lubricants on the density of the composites is clearly seen because other factors (process parameters and, the type and amount of constituents) are similar for all the composites. The M type composite (MoS_2 reinforced) has the highest density among the composites. It is primarily because of the high density of MoS_2 (ρ = 5.06 g/cc). Also, lubricants control the densification by influencing the compaction and sintering characteristics of the composites. This fact is apparent from the pore fraction (densification) values of the composites. While comparing the pore fraction, the low pore fraction/high densification value of a M type composite indicates that the MoS_2 provides relatively less obstruction to the compaction and sintering than other two composites (h-BN (B) type and graphite (G) type).

Table 6
Properties of the composites.

Properties	G	B	M
Theoretical density (g/cc)	7.56	7.55	7.85
Average experimental density (g/cc)	7.22	7.15	7.62
Average pore fraction (%)	4.457	5.337	2.88
Average hardness (BHN)	80 ± 7	75 ± 6	104 ± 3
Average surface roughness, Ra (μm)	1.15 ± 0.15	1.03 ± 0.37	0.57 ± 0.3

The M type composite has the highest hardness among the composites. The low porosity content, high compressive strength of the MoS_2 (perpendicular to the basal plane), the hard and thin MoO_3 outer layer on the MoS_2 enhance the hardness of a M type composite [41].

The M type composite has the lowest surface roughness (R_a) among the composites. The shear strength of MoS_2 is very low along the layers resulting in an easy flow over the surface during the machining. Thus, the better spreading or coverage of the MoS_2 over the surface of the composite results in improved surface finish. Ramesh and Suresha [42] reported a similar finding in the carbon-epoxy hybrid composites reinforced with MoS_2.

3.2. Wear behavior

The wear loss of the composites for various speeds and loads is presented in Fig. 4. First, we look at the effect of sliding speeds on the wear loss of the composites. The wear loss (by mass) of the B and G type composites increases linearly with the sliding speed. In contrast, the wear loss increases up to 6 m/s and then slightly decreases for M type composites. The steep slope of the wear loss curve with the sliding speeds indicates that the wear loss rate is highest for the G type composites. This behavior is attributed to the loss of graphite with increasing sliding speeds. The frictional temperature rise with the sliding speed causes decomposition of the graphite resulting in huge wear loss. The macrograph of the G type composites tested at 9 m/s and 900 N, as given in Fig. 5(a), shows the absence of graphite on the surface supporting the above proposition. Further, the macrograph shows isolated pockets of oxide regions. The presence of shallow cavities and thermal cracks on the surface makes the surface oxidation non uniform. These cavities and cracks are the result of removal of the reinforcements (silica and graphite) from the surface during the wear. From the above features,it can be suggested that the combination of wear mechanisms (abrasive, delamination, oxidation) is operative at 9 m/s in the G type composites.

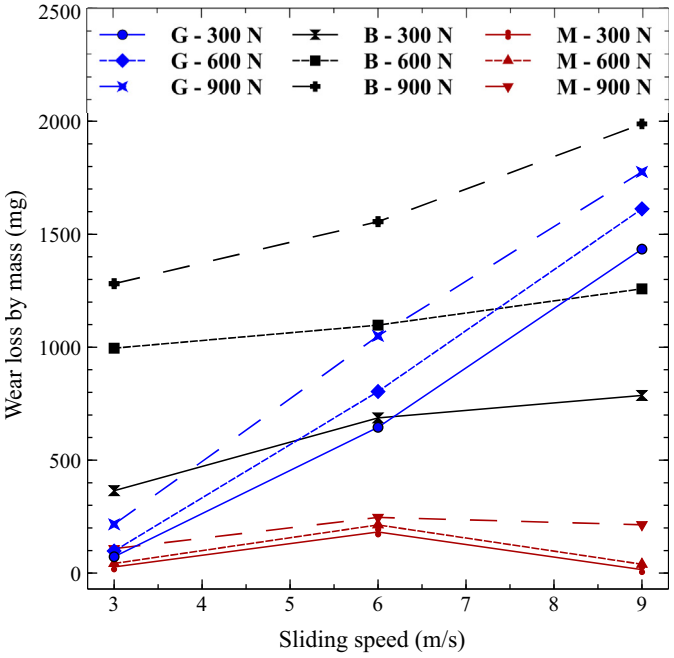

Fig. 4. Wear loss by mass (g) of the composites.

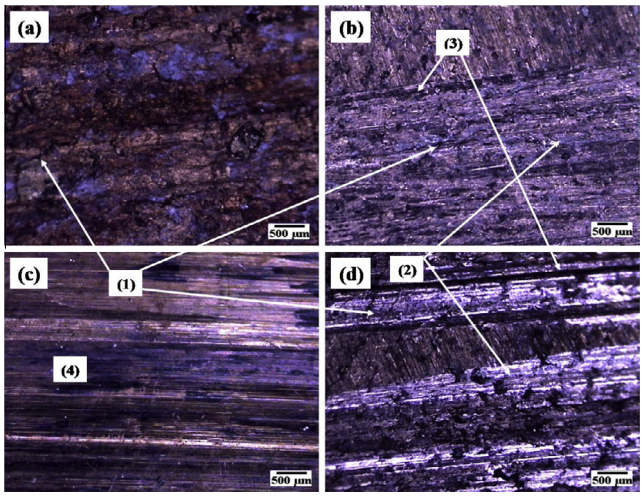

Fig. 5. Wear surface morphology of the (a) G type composite tested at 9 m/s and 900 N, (b) B type composite tested at 3 m/s and 900 N, (c) M type composite tested at 9 m/s and 600 N, and (d) B type composite tested at 9 m/s and 900 N. (1) thermal cracks, (2) oxide scale, (3) groove lines, and (4) tribofilm layer.

Next, we look at the effect of braking loads on the wear loss of the composites. The wear loss increases with the braking load for any case of sliding speed and composite type combinations. The friction increases with increasing braking load because of the increase in the real area of contact between the sliding couple, that in turn raises the friction induced temperature at the contact interface. The contact surface temperature rise and high friction promote faster wear of the pad material by oxidation and softening effects and the easy material plowing by counter surface asperities. Compared to other composites, the braking load effects are severe for B type composites. The macrograph of the B type composites tested at 3 m/s and 900 N, as shown in Fig. 5(b), shows abrasive groove lines and cracks with little oxidation supporting the above explanation. The high braking load is concentrated on the silica particles by the load sharing mechanism. However, observed cracked particles in the B type composites (as seen in Fig. 3(b)) do not help in supporting the braking load. In addition, the high stress concentration is generated at the particle/matrix interfaces by the high dislocation density. These dislocations are formed by the differential thermal contraction of the matrix and particles during the sintering process. The application of braking load removes easily these particles resulting in the void formation. Voids and cracked particles are potential sites for crack nucleation. The propagation of cracks usually takes place by linking the voids in the sliding direction by the barber effect (thermoelastic and plastic instabilities in the sliding) [43]. Thus, the wear loss is considerably increased by the removal of sheets of material and particle pull-out with the braking load in the B type composites.

The M type composite has the least wear loss (best wear resistance) than other composites for any combination of sliding speed and load conditions. It indicates that MoS_2 plays a key role in controlling the wear loss of the composites. The MoS_2 has the ability to form a uniform tribolayer, as observed from Fig. 5(c), that helps in reducing the friction and wear loss at higher speed and load conditions. Further, the stability of MoS_2 is better because of the lower oxidation rate due to the presence of the outer oxidized layer in the layer structure of MoS_2 [41]. Also, high hardness and densification, and low surface roughness of the M type composites contribute to the improvement of the wear resistance. Particularly, low surface roughness (R_a) helps in reducing the wear and friction of the M type composites at low sliding speed and load conditions. The low R_a gives the smooth surface and hence, the probability of the interlocking of the asperities andsubsequent shearing failure during wear is relatively lower resulting in minimal wear loss and friction. The decreasing wear loss of the M type composites from 6 to 9 m/s at 300 and 600 N loads may be due to the complete and uniform coverage of tribofilm, as observed in Fig. 5(c), and the absence of the third body wear.

Finally, we look at the wear mechanism operating at different speed and load conditions in the composites. In order to identify the probable wear mechanisms, B type composites were selected. The macrographs of the composites tested at 900 N for the case of 3 and 9 m/s are shown in Fig. 5(b) and (d). At low sliding speed (3 m/s), the effect of temperature is less significant. Therefore, mechanical forces decide the wear mechanism. The observation of continuous, thin, shallow surface depression in the sliding direction indicates that the counter surface asperities plowed the composite surface resulting in abrasive wear. With increasing speed, the effects of oxidation, particle delamination, and thermal assisted fatigue increase, as observed from Fig. 5(d). Surface oxides have low bonding strength with the substrate facilitating easy separation. The preexisting surface asperities and the abrasive grooves concentrate the braking load at discrete points resulting in the non uniform distributions of friction and friction induced temperature. That causes mechanical and thermal disturbances resulting in the removal of thin wear sheets during the wear. Apart from the thermal softening, the increasing sliding speed enhances the shear rate of the contact surfaces resulting in the sudden fracture of surface materials [44]. The coupled effects of temperature and mechanical forces accelerate the wear loss. At higher sliding speeds (6–9 m/s), the multiples of wear mechanisms (oxidation, delamination, abrasion, and thermal assisted fatigue) are operating simultaneously. The relative contribution of each mechanism is difficult to quantify because of the complexity of the wear process and solid lubricant effects, and the simultaneous operation.

3.3. Statistical analysis

A statistical analysis based on the multivariate analysis of variance (ANOVA) technique was performed to understand the influence of the solid lubricant, braking load and speed on the wear

Table 7
Analysis of variance (ANOVA) table for composites (df – degree of freedom, SS – sum of squares, MS – mean of squares).

Source	df	SS	Adjusted SS	Adjusted MS	*F* ratio	*P* value	% Contribution
X	2	4,770,670	4,770,670	2,385,335	386.23	0.000	47
L	2	992,312	992,312	496,156	80.34	0.000	9.78
S	2	1,953,239	1,953,239	976,619	158.13	0.000	19.24
X ∗ *L*	4	650,721	650,721	162,680	26.34	0.000	6.41
X ∗ *S*	4	1,692,662	1,692,662	423,165	68.52	0.000	16.68
L ∗ *S*	4	41,295	41,295	10,324	1.67	0.248	0.41
Error	8	49,408	49,408	6176	–	–	0.49
Total	26	10,150,307	–	–	–	–	100

S = 78.5877, *R*-Sq = 99.51% and *R*-Sq(adj) = 98.42%.

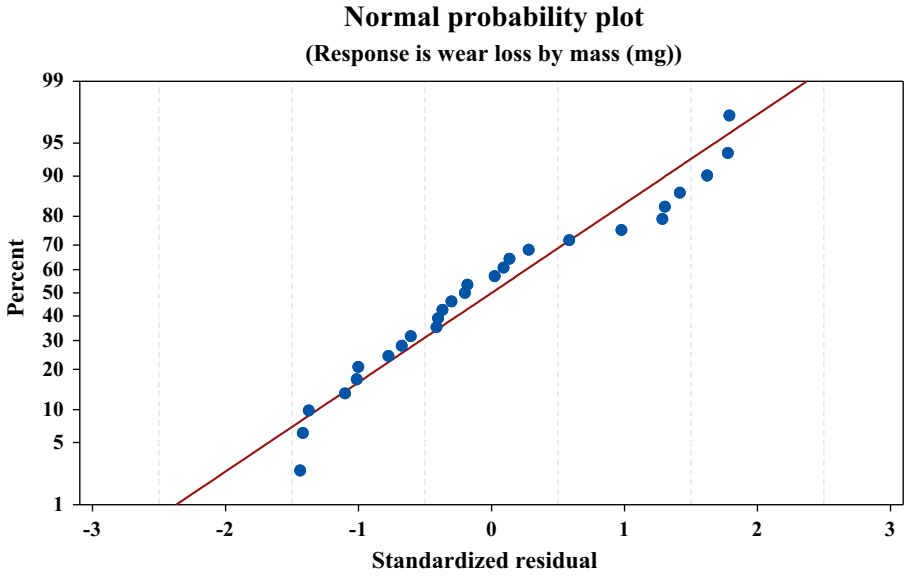

Fig. 6. Normal probability plot of standardized residuals of the wear loss data.

behavior of composites. Table 7 gives the results of ANOVA. Before discussing the ANOVA results, it is important to validate the model assumptions. The assumptions are that (1) the response(wear) data are normally distributed and independent, and the residuals are not normal, (2) the response data have constant variance for all the settings of input variables, and the errors are unbiased.

To verify the first assumption, the normal probability of wear response data is plotted which is shown in Fig. 6. Most of the data fall very close to the straight line fit confirming the normality assumption. The residuals were plotted with respect to the fitted values and the input variables to verify the second assumption. The residual plots are shown in Figs. 7 and 8.

The observations of random distribution of the residuals about to zero (as observed in Fig. 7) and, no systematic pattern in the residuals (as seen in Fig. 8) validate the second assumption of constant variance. The standardized residuals are found to be less than 3, as seen from Fig. 8. Also, there are no observations of predominantly positive or negative residuals, or uneven data spreading in Fig. 8. The above observations indicate that the data set contains no outliers.

Table 7 gives the statistically significant factors affecting the wear resistance based on their *P* values (probability of significance). The factors whose *P* values are less than 0.05% (95% confidence levels) are generally regarded as statistically significant. Based on this criterion,it is found that solid lubricants (*X*), load (*L*), speed (*S*), the interaction of X×L, and the interaction of X×S are statistically significant. Among these factors, lubricants have the greatest effect in influencing the wear loss, as observed from the highest % contribution (47%). Next, braking speed (19%), and the interaction between X×S (17%) have second and third rank influences respectively on the wear loss. The braking load (<10%) and other interaction combinations (<8%) do not have much influence on the wear loss. It is important to note that the contribution of error in our model is 0.49%. While compared to the error value, the % contribution of load and speed interaction (0.41%) is much lesser indicating no physical significance of the factor [45].

Response tables of wear loss means and *S*/*N* ratio for composites are presented in Tables 8 and 9. Both the tables show that the solid lubricant is the most significant factor deciding the wear resistance of the composites. Further, the ranking of the factors controlling the wear loss is found to be in the following order: solid lubricant > speed > load. These results are in agreement with the ANOVA results.

The interaction plot for wear loss means of the composites is given in Fig. 9. The sharp drop of the slope from G to M point in the material column indicates that the MoS_2 has the greatest effect in improving the wear resistance of the composites. Comparing the interaction between the factors, the load and speed interaction has a low and unchanging slope between data points. It implies that the load and speed interaction has the least influence on the wear loss.

The main effects plot for wear loss means of the composites is given in Fig. 10. The data points in the material column follow a negative trend indicating that the wear resistance increases from h-BN to MoS_2 lubricants. Hence, the MoS_2 is the best amongst the lubricants. Both the speed and the load have positive slopes

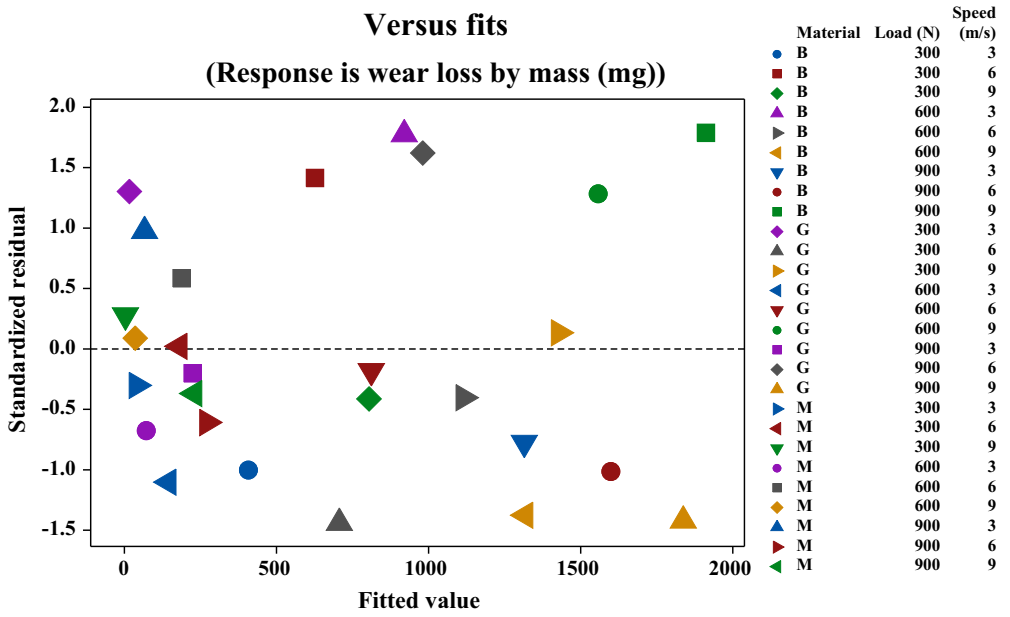

Fig. 7. Variation of the standardized residuals with fitted values of the wear loss data.

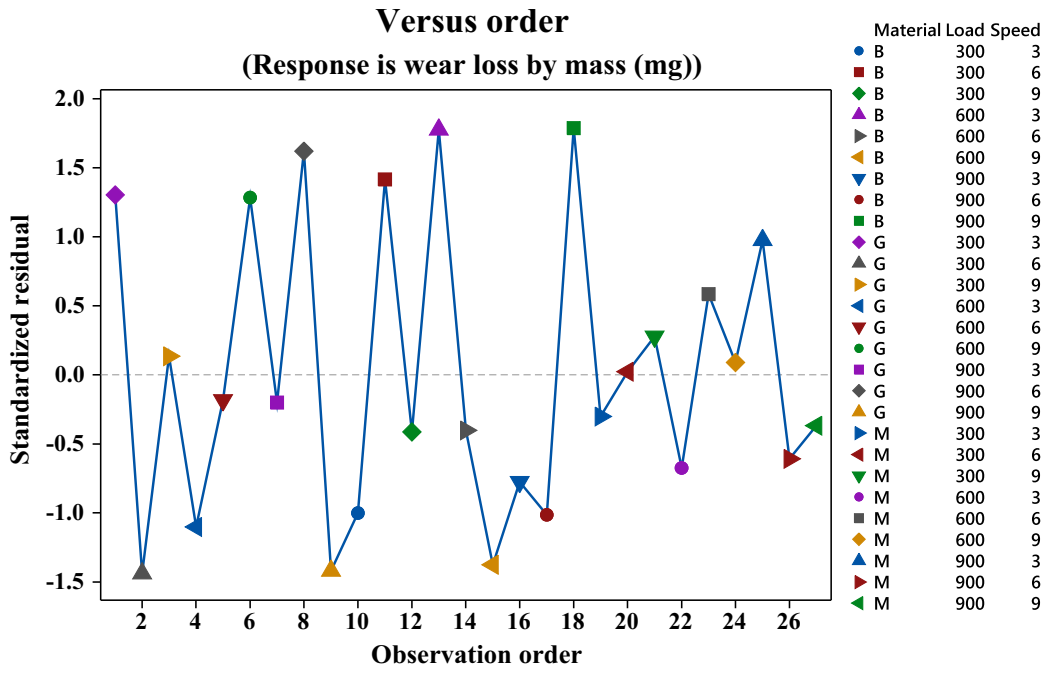

Fig. 8. Variation of the standardized residuals with observed order values of the wear loss data.

indicating that the increase of these factors enhances the wear loss of the composites. These results are in agreement with other reports [12]. Between the speed and the load, the speed has relatively higher positive slope than the load indicating its stronger effects on the wear resistance of the composites.

The response surface analysis was also carried out to compare the model results. The three dimensional surface plots showing the interaction effects of lubricants, load, and speed are shown in Fig. 11. It is clear from the slope of the planes that solid lubricants influence significantly wear resistance of the composites. The slope of the load and speed interaction is relatively lower indicating its least significance. These results are in agreement with the ANOVA results.

3.4. Braking behavior

The braking performance of the composites is usually evaluated based on the friction coefficient (CoF) and stopping distance (or time) values. The data acquisition system in a brake dynamometer records the mean torque (T) and the stopping distance. The CoF (μ) is calculated from the mean brake torque data ($T = \mu *$ braking load $*$ radial distance from the centroid of the disc to the composite center). The variations of CoF, mean torque, and stopping distance of the composites for different sliding speeds and loads are shown in Figs. 12–14. It is clear that the plots of CoF and mean torque appear similar because the CoF is derived from the mean torque data.

Table 8
Wear loss (mass) response table for means: smaller the better.

Level	X	L	S
1	7708.35	4214.05	3206.05
2	10014.85	6161.95	6481.90
3	1088.95	8436.15	9124.20
Δ	8925.9	4222.1	5918.15
Rank	1	3	2

Table 9
S/*N* response table for wear loss: smaller the better.

Level	X	L	S
1	−60.07	−46.66	−44.34
2	−54.52	−50.66	−55.08
3	−38.20	−55.47	−53.36
Δ	21.87	8.8	10.74
Rank	1	3	2

First, we look at the effect of sliding speed on the braking performance of the composites. The CoF or braking torque increases with the sliding speed for both M type and B type composites, whereas it increases up to a critical speed of 6 m/s and then decreases for G type composites. The brake fade causes the reduction of CoF after 6 m/s in the graphite reinforced composite (G type). The increase in contact surface temperature (brake energy dissipation) with increasing braking speed causes the brake fade. The increase in the brake interface temperature oxidizes the graphite into CO_2 and consequently, degrades the lubricity of the tribofilm resulting in lower braking torque or CoF [27]. In addition to the graphite oxidation, the matrix (Cu) also gets oxidized at high contact temperature. The coverage of oxide scale increases with increasing contact temperature. The presence of oxide scale at the contact surface decreases the friction at the interface by reducing metal–metal adhesive bonding between the contact couples due to the dissimilar material characteristics [17] and by reducing the asperities interlocking (abrasive) between contact surfaces by smoothening the surface. Also, at higher sliding speed, the third body wear particles contribution to the friction improvement gets reduced due to rapid removal from the contact interface [17,46]. Further, the increasing braking load intensifies the brake fade effect. For instance, the G type composite tested at extreme speed and load (9 m/s and 900 N) condition shows significant reduction in braking torque or CoF indicating the very high brake fade effects. This result also suggests that the tribofilm formed by the graphite is not stable beyond 6 m/s because of the interaction between the graphite and oxides [47]. At any load condition, the slope of the braking torque (as seen in Fig. 12) from 3 to 6 m/s is higher than that of the braking torque from 6 to 9 m/s for all the composites. It points out the fact that the improvement of friction or braking torque beyond 6 m/s is not much because the stability of the friction improving tribofilm is disturbed by the increasing friction temperature rise. Both the mean torque and the CoF have the average error percent of 9%, 16%, and 30% at 3 m/s, 6 m/s, and 9 m/s respectively for the G type composite. Other two composites (B type and M type composites) have the average error percent of 10%, 14%, and 21%, and 11%, 17%, and 21% respectively at 3 m/s, 6 m/s, and 9 m/s. The high error bar percent value at 9 m/s supports the above explanation. Among the composites, the G type composite provides the highest braking torque or CoF at 3 m/s for all the loading conditions. The presence of adsorbed vapors in the graphite helps in providing high friction at low speed (3 m/s) condition. At higher speeds, the adsorbed vapors get removed by increasing friction temperature resulting in loss of lubricity. By taking into consideration of the error bars, it is found that there is not much difference in the braking torque or CoF among the composites at higher speeds (>3 m/s) for all the loading conditions.

The stopping distance (time) increases with the sliding speed for all the composites, as seen in Fig. 14. The G type composite has the average error percent of 10%, 17%, and 31% at 3 m/s, 6 m/s, and 9 m/s respectively in the stopping distance. Other two composites (B type

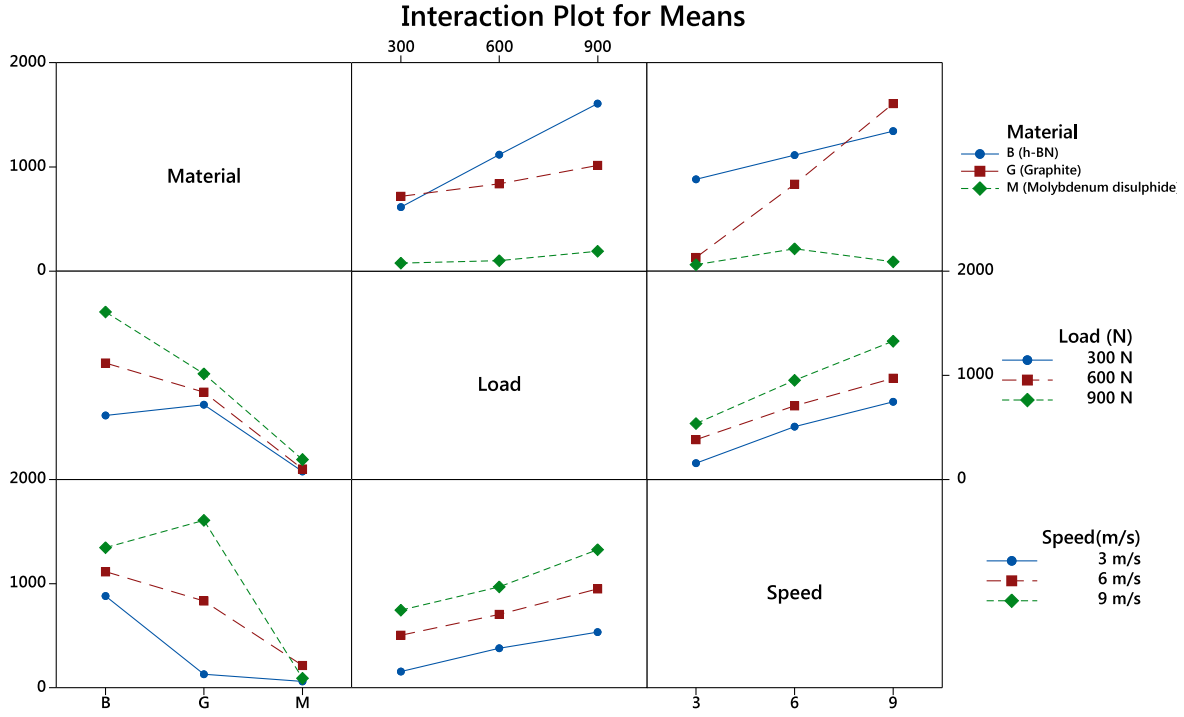

Fig. 9. Interaction plots for wear loss means of the composites.

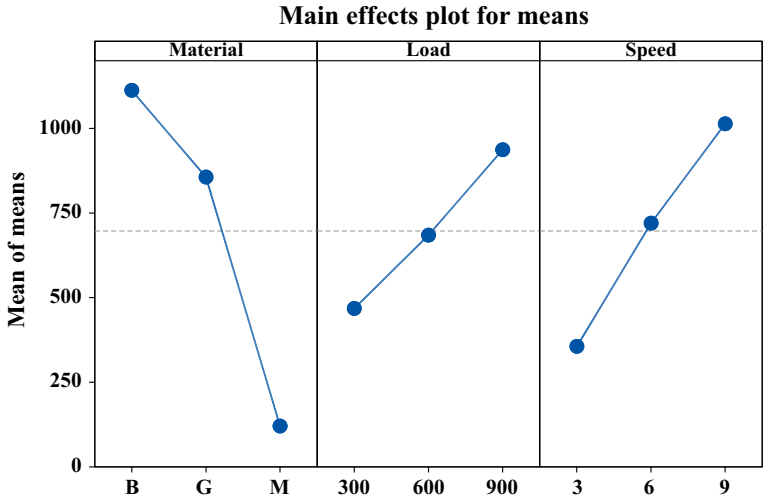

Fig. 10. Main effects plot for wear loss means of the composites. (Units of load and speed are in N and m/s respectively.)

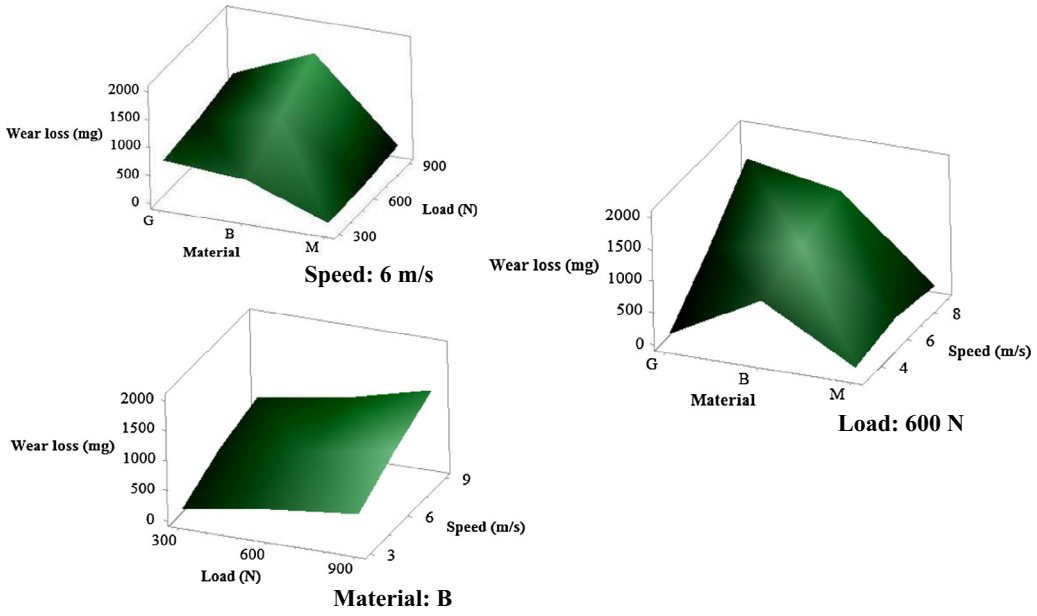

Fig. 11. Response surface plots for the wear loss of the composites.

and M type composites) have the average error percent of 9%, 17%, and 29%, and 7%, 13%, and 28% respectively at 3 m/s, 6 m/s, and 9 m/s. At 3 and 6 m/s, the difference in the stopping distance among the composites is not appreciable for all the loading conditions and hence, they can be considered to have a nearly equal braking performance. At 9 m/s, the M type composite provides less stopping distance for 300 N condition, whereas the B type composite provides less stopping distance for 600 and 900 N conditions.

Now, let us look at the effect of braking load on the braking performance of the composites. The braking torque increases with increasing load at any particular sliding speed for all the composites. The increasing load enhances the mating surfaces contact points and improves the braking torque. There is no increasing/decreasing trend of COF with increasing load observed, as seen in Fig. 13. For example, the variation of CoF with increasing load at 6 and 9 m/s is almost the same whereas there is a considerable change from 600 to 900 N at 3 m/s for G and M composites. For the B composite, increasing load increases the CoF at 3 m/s whereas the CoF is almost the same for increasing load from 300 to 600 N at 6 and 9 m/s. From these observations, it is understood that the CoF is influenced by many factors. These factors include oxide scale, change in the tribofilm chemistry, decomposition of the tribofilm constituents, frictional heating, and third body wear trapped in between the sliding couple. They complicatedly affect the number and strength of asperities in contact resulting in non uniform trend of CoF. While comparing the slope of the braking torque line with increasing load for 3 and 6 m/s conditions (the plot is not shown here but can be constructed from Fig. 12), it is found that the effect of load on improving braking torque increases for all the composites but at the cost of high wear loss. The change in the wear mechanism (from abrasive to tribofilm and oxidation wear) is attributed to the above effect. In contrast, there is no much change in the slope with increasing load at 9 m/s indicating the complex interaction of wear mechanisms. Among the composites, both B and M type composites show consistent improvement in the braking torque with increasing load at any sliding speed conditions. The G type composite shows reduced braking torque with increasing speed from 6 m/s to 9 m/s at 900 N. At 300, 600 and

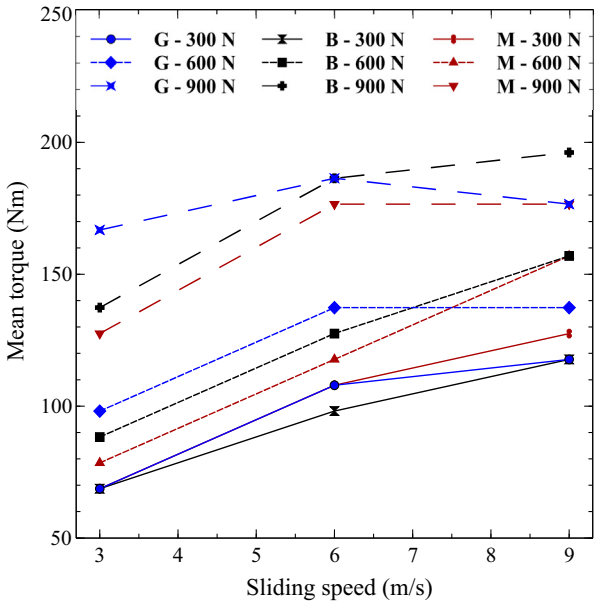

Fig. 12. Effect of braking speed on mean torque of the composites (total braking stops: 50), error bar values for 9 m/s – G300: ±39, G600: ±39, G900: ±49, B300: ±39, B600: ±19, B900: ±39, M300: ±29, M600: ±39, M900: ±29.

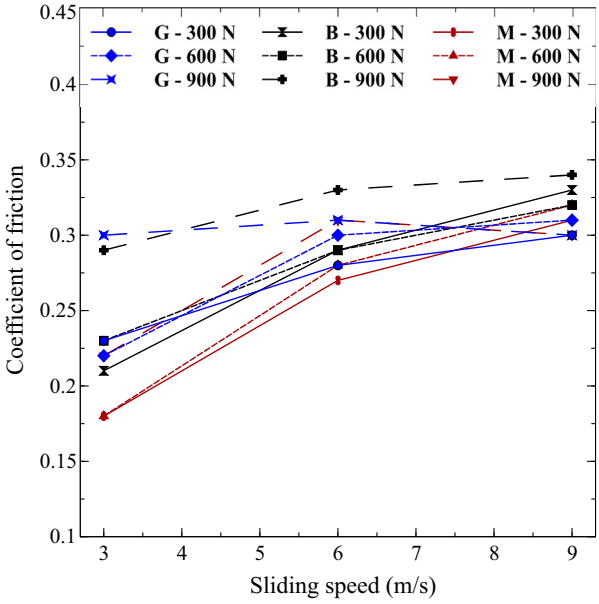

Fig. 13. Effect of braking speed on mean friction coefficient of the composites (total braking stops: 50), error bar values for 9 m/s – G300: ±0.09, G600: ±0.09, G900: ±0.095, B300: ±0.08, B600: ±0.05, B900: ±0.08, M300: ±0.06, M600: ±0.075, M900: ±0.06.

900 N, the G type composite provides relatively higher braking torque for 3 m/s. Considering the error bar values, both M and B type composites provide nearly similar braking performance at higher speed (6–9 m/s) and load (900 N) conditions. The mean stopping distance (time) decreases with increasing load for all the composites except for the M type composite. The stopping distance increases from 300 N to 600 N at 6 m/s in the M type composite. This deviation from the trend is probably due to the role of third body wear. The third body wear particles trapped in between the sliding interfaces may have got removed during sliding. The stopping power due to the abrasion of the third body wear gets reduced

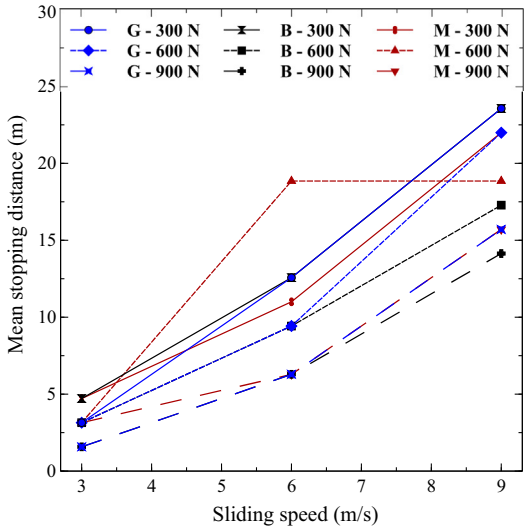

Fig. 14. Effect of braking speed on mean stopping distance of the composites (total braking stops: 50), error bar values for 9 m/s – G300: ±6, G600: ±6, G900: ±8, B300: ±1.5, B600: ±3, B900: ±3, M300: ±4, M600: ±4, M900: ±6.

and hence, there is an increase in the stopping distance. However, the exact reason for this anomaly needs further investigation.

4. Conclusions

Three types of Cu/silica composites based on the solid lubricants (graphite, h-BN, and MoS_2) addition were processed using the powder metallurgy. The composites were tested to study the influence of solid lubricants, braking load, and sliding speed on the wear behavior of the Cu/silica composites.

A summary of the key insights of the results is given below:

- The MoS_2 reinforced composite possesses higher density, densification, hardness and lower surface roughness.
- The microstructural characterization of the composites shows that the interfaces of silica and the matrix are smooth and free from interfacial reaction products, and the distribution of the silica and solid lubricants is uniform in the copper matrix.
- MoS_2 is the most effective lubricant in improving the wear resistance of the composites at any sliding speed and load combinations. The wear surface morphology studies show that abrasive wear is significant at 3 m/s. At higher speeds (>3 m/s), many wear mechanisms (oxidation, delamination, thermal assisted fatigue and abrasion) are found to occur.
- The statistical analysis based on the multivariate ANOVA techniques explains well the experimental results with a reasonable accuracy (error < 1%). The analysis shows that the solid lubricant is the most dominant factor deciding the wear resistance of the composites.
- Response tables of wear loss means and *S*/*N* ratio for the composites rank the significance of the factors controlling the wear loss in the following decreasing order: solid lubricants, sliding speed, and braking load.
- The ranking of solid lubricants from the statistical analysis gives the following order of excellence: MoS_2, graphite, and h-BN in improving the wear resistance of the composites.
- The graphite reinforced composite provides higher braking performance at 3 m/s for all the loading conditions. Considering the error bar values, both the h-BN and MoS_2 reinforced composites provide better braking performance among the composites at higher speed (>3 m/s) and load (>300 N) conditions.

Acknowledgments

I gratefully acknowledge Prof. Srikanth Vedantam, Department of Engineering Design, IIT Madras for his technical and language guidance. I also thank the anonymous reviewers for their detailed comments.

References

[1] T.L. Ho, M.B. Peterson, Development of Aircraft Brake Materials, Rensselaer Polytechnic Institute, Troy, New York, 1974 (Report No. NASA CR 134663).
[2] T.L. Ho, M.B. Peterson, F.F. Ling, Effect of frictional heating on brake materials, Wear 30 (1974) 73–91.
[3] M. Asif, K. Chandra, P.S. Misra, Development of iron based brake friction material by hot powder preform forging technique used for medium to heavy duty applications, J. Min. Mater. Charact. Eng. 10 (3) (2011) 231–244.
[4] V.S. Arunachalam, O.V. Roman, Powder Metallurgy: Recent Advances, Oxford & IBB Publishing Co., New Delhi, 1989. ISBN: 185529009X.
[5] T.R. Prabhu, V.K. Varma, S. Vedantam, Tribological and mechanical behavior of multilayer Cu/SiC + Gr hybrid composites for brake friction material applications, Wear 317 (2014) 201–212.
[6] W.H. Hunt, Applications of metal matrix composites, Encyclopedia Mater. Sci. Technol. (2001) 5442–5447.
[7] D.D.L. Chung, Composite Materials, Science, and Applications: Functional Materials for Modern Technologies, Springer, Great Britain, London, 2004 (ISSN 1619-0181).
[8] P. Yao, H. Sheng, X. Xiong, B. Huang, Worn surface characteristics of Cu-based powder metallurgy bake materials for aircraft, Trans. Nonferr. Met. Soc. China 17 (1) (2007) 99–103.
[9] P.J. Blau, Compositions, Functions and Testing of Friction Brake Materials and Their Additives. Report No. ORNL/TM-2001/64, U.S. Department of Energy, 2001.
[10] S.P. Sapate, A. Uttarwar, R.C. Rathod, R.K. Paretkar, Analyzing dry sliding wear behaviour of copper matrix composites reinforced with pre-coated SiCp particles, Mater. Des. 30 (2009) 376–386.
[11] C.S. Ramesh, R.N. Ahmed, M.A. Mujeebu, M.Z. Abdullah, Development and performance analysis of novel cast copper–SiC–Gr hybrid composites, Mater. Des. 30 (2009) 1957–1965.
[12] V.S. Aigbodion, S.B. Hassan, Experimental correlations between wear rate and wear parameter of Al–Cu–Mg/bagasse ash particulate composite, Mater. Des. 31 (2010) 2177–2180.
[13] S. Koksal, F. Ficici, R. Kayikci, O. Savas, Experimental optimization of dry sliding wear behavior of in situ AlB_2/Al composite based on Taguchi's method, Mater. Des. 42 (2012) 124–130.
[14] T.S. Kiran, M.P. Kumar, S. Basavarajappa, B.M. Viswanatha, Dry sliding wear behavior of heat treated hybrid metal matrix composite using Taguchi techniques, Mater. Des. 63 (2014) 294–304.
[15] Y. Sahin, K. Ozdin, A model for the abrasive wear behaviour of aluminum based composites, Mater. Des. 29 (2008) 728–733.
[16] Y. Sahin, Optimal testing parameters on the wear behaviour of various steels, Mater. Des. 27 (2006) 455–460.
[17] M. Nosonovsky, P.K. Rohatgi, Biomimetics in Materials Science: Self-healing, Self-lubricating, and Self-cleaning Materials, Springer Series in Materials Science, New York, 2012. pp. 195–236.
[18] P.K. Rohatgi, B.F. Schultz, A. Daoud, W.W. Zhang, Tribological performance of A206 aluminum alloy containing silica sand particles, Tribol. Int. 43 (2010) 455–466.
[19] Y.C.M. Kumar, U. Shankar, Evaluation of mechanical properties of aluminum alloy 6061-glass particulates reinforced metal matrix composites, Int. J. Mod. Eng. Res. 2 (5) (2012) 3207–3209.
[20] M. Sayuti, S. Sulaiman, T.R. Vijayaram, B.T.H.T. Baharudin, M.K.A. Arifin, Manufacturing and properties of quartz (SiO_2) particulate reinforced Al–11.8%Si matrix composites, in: N. Hu (Ed.), Composites and Their Properties, InTech, 2012, pp. 411–436 (ISBN 978-953-51-0711-8).
[21] J. Pelleg, Reactions in the matrix and interface of the Fe–SiC metal matrix composite system, Mater. Sci. Eng. A 269 (1999) 225–241.
[22] Y. Yasutomi, J. Sawada, T. Kikuchi, K. Nakamura, Y. Manabe, K. Nagano, H. Kuroda, T. Sumi, H. Kubokawa, M. Nagai, H. Kogure, Y. Sawai, T. Kishi, Effects of the SiC/Al interface reaction on fracture behavior of a composite conductor using SiC fiber reinforced aluminum for next generation power equipment, J. Mater. Sci. 34 (7) (1999) 1583–1593.
[23] J. Pelleg, M. Ruhr, M. Ganor, Control of the reaction at the fibre–matrix interface in a Cu/SiC metal matrix composite by modifying the matrix with 2.5 wt.% Fe, Mater. Sci. Eng. A 212 (1996) 139–148.
[24] J. Hemanth, Quartz (SiO_2p) reinforced chilled metal matrix composite (CMMC) for automotive applications, Mater. Des. 30 (2009) 323–329.
[25] K.H.W. Seah, J. Hemanth, S.C. Sharma, Mechanical properties of aluminum/quartz particulate composites cast using metallic and non-metallic chills, Mater. Des. 24 (2) (2003) 87–93.
[26] S. Sulaiman, M. Sayuti, R. Samin, Mechanical properties of the as-cast quartz particulate reinforced LM6 alloy matrix composites, J. Mater. Process. Technol. 201 (2008) 731–735.
[27] M.H. Cho, J. Ju, S.J. Kim, H. Jang, Tribological properties of solid lubricants (graphite, Sb_2S_3, MoS_2) for automotive brake friction materials, Wear 260 (2006) 855–860.
[28] S. Suresha, B.K. Sridhara, Effect of addition of graphite particulates on the wear behaviour in aluminum–silicon carbide–graphite composites, Mater. Des. 31 (4) (2010) 1804–1812.
[29] L.G. Hoyer, A. Bach, G.T. Nielsen, P. Morgen, Tribological properties of automotive disc brakes with solid lubricants, Wear 232 (1999) 168–175.
[30] N. Axen, S. Jacobson, A model for the abrasive wear resistance of multiphase materials, Wear 174 (1994) 187–199.
[31] G.Y. Lee, C.K. Dharan, R.O. Ritchie, A physically-based abrasive wear model for composite materials, Wear 252 (3–4) (2002) 322–331.
[32] K. Song, J. Xing, Q. Dong, P. Liu, B. Tian, X. Cao, Optimization of the processing parameters during internal oxidation of Cu–Al alloy powders using an artificial neural network, Mater. Des. 26 (2005) 337–341.
[33] V.D. Tsoukalas, Optimization of porosity formation in AlSi(9)Cu(3) pressure die casting using genetic algorithm analysis, Mater. Des. 29 (2008) 2027–2033.
[34] E.J. Femandez, F.M. Rocio, R.V. Diaz, R.T. Navarro, Abrasive wear analysis using factorial experiment design, Wear 255 (2003) 38–43.
[35] M. Bayhan, K. Onel, Optimization of reinforcement content and sliding distance for AlSi(7)Mg/SiCp composites using response surface methodology, Mater. Des. 31 (2010) 3015–3022.
[36] O.P. Modi, R.P. Yadav, D.P. Mondal, R. Dasgupta, S. Das, Abrasive wear behaviour of zinc–aluminum alloy–10% Al_2O_3 composite through factorial design of experiment, J. Mater. Sci. 36 (2001) 1601–1607.
[37] G. Taguchi, S. Konishi, Taguchi Methods, Orthogonal Arrays and Linear Graphs, Tools for Quality Engineering, American Supplier Institute, Dearborn, MI, 1987. pp. 35–38.
[38] G. Taguchi, Taguchi on Robust Technology Development Methods, ASME Press, New York, NY, 1993. pp. 1–40.
[39] T.R. Prabhu, V.K. Varma, S. Vedantam, Effect of reinforcement type, size, and volume fraction on the tribological behavior of Fe matrix composites at high sliding speed conditions, Wear 309 (1–2) (2014) 247–255.
[40] T.R. Prabhu, V.K. Varma, S. Vedantam, Effect of SiC volume fraction and size on dry sliding wear of Fe/SiC/graphite hybrid composites for high sliding speed applications, Wear 309 (1–2) (2014) 1–10.
[41] W.O. Winer, Molybdenum disulphide as a lubricant: a review of the fundamental knowledge, Wear 10 (1967) 422–452.
[42] B.N. Ramesh, B. Suresha, Optimization of tribological parameters in abrasive wear mode of carbon-epoxy hybrid composites, Mater. Des. 59 (2014) 38–49.
[43] J.R. Barbar, Thermoelastic instabilities in the sliding of conforming solids, Proc. Roy. Soc. 112 (A) (1969) 181–394.
[44] A. Chowdhury, M.K. Khalil, D.M. Nuruzzaman, M.L. Rahaman, The effect of sliding speed and normal load on friction and wear property of aluminum, Int. J. Mech. Mechatron. Eng. 11 (2011) 45–49.
[45] S. Basavarajappa, G. Chandramohan, J.P. Davim, Application of Taguchi techniques to study dry sliding wear behaviour of metal matrix composites, Mater. Des. 28 (2007) 1393–1398.
[46] P.J. Blau, ASM Handbook, 10th ed., Friction, Lubrication, and Wear Technology, vol. 18, ASM International Materials Park, OH, 1992.
[47] H.E. Sliney, Solid lubricant materials for high temperatures – a review, Tribol. Int. 15 (5) (1982) 303–315.